Journal of Materials Chemistry

Cite this: J. Mater. Chem., 2012, 22, 13174

www.rsc.org/materials

PAPER

A simple and efficient approach to synthesize amidoborane ammoniates: case study for $Mg(NH_2BH_3)_2(NH_3)_3$ with unusual coordination structure†

Xiangdong Kang,[a] Hui Wu,*[bc] Junhong Luo,[a] Wei Zhou[bc] and Ping Wang*[a]

Received 3rd March 2012, Accepted 26th April 2012
DOI: 10.1039/c2jm31326j

Metal amidoborane ammoniates are a new type of promising hydrogen storage material consisting of metal cation, $[NH_2BH_3]^-$ anionic unit and NH_3 ligand. Herein, we report a new reactive ball milling approach for preparation of magnesium amidoborane ammoniate, $Mg(NH_2BH_3)_2(NH_3)_3$. Our study found that mechanically milling the NH_3BH_3–MgH_2 mixture in a 2 : 1 molar ratio under NH_3 atmosphere can readily produce $Mg(NH_2BH_3)_2(NH_3)_3$. Its crystal structure was successfully determined by a combination of X-ray diffraction (XRD) analysis and first-principles calculations. This compound possesses a novel ordered structure with alternating layers of $Mg(NH_3)_6^{2+}$ hexamminemagnesium cations and $Mg(NH_2BH_3)_4^{2-}$ complex anions, in which Mg^{2+} exhibits both VI and IV coordinations. Property measurements found that $Mg(NH_2BH_3)_2(NH_3)_3$ can release 7 equivalents (10.6 wt%) of H_2 upon heating to 300 °C in a closed system. A combination of XRD, Fourier transformation infrared spectroscopy (FTIR), and solid-state ^{11}B MAS NMR techniques has been employed to characterize $Mg(NH_2BH_3)_2(NH_3)_3$ and its dehydrogenation product. A series of control experiments have also been conducted to gain insight into the formation mechanism of $Mg(NH_2BH_3)_2(NH_3)_3$.

1. Introduction

The development of hydrogen-fueled vehicles and portable electronics requires advanced hydrogen storage materials that can store and deliver large amounts of hydrogen at a moderate temperature with fast kinetics.[1] Recently, ammonia borane (NH_3BH_3, AB for short) has received considerable attention as a potential hydrogen storage medium. AB is a unique molecular solid with exceptionally high hydrogen density and moderate thermal stability and particularly, it represents a new class of single-phase materials that contain simultaneously protonic and hydridic hydrogen.[2–4] In past years, the strategies of nano-confinement using scaffolds,[5–8] additive promotion[9–13] and chemical modification have been employed and proven to be effective for promoting H_2 release and for suppressing volatile byproducts from AB. In particular, the successful implementation of the chemical modification strategy has given rise to a wealth of new materials,[14] *e.g.*, metal amidoboranes,[15–22] metal amidoborane ammoniates,[23–25] and ammonia borane borohydride complexes,[27] which exhibited improved dehydrogenation properties relative to pristine AB.

Metal amidoborane ammoniates are a new type of coordination compound consisting of metal cation, $[NH_2BH_3]^-$ anionic unit and NH_3 ligand. As the hydrogen density of NH_3 is as high as 17.8 wt%, the ammoniates typically possess intriguingly high hydrogen densities.[26] Owing to the competitive deammoniation reaction, the deliverable H_2 amount from metal amidoborane ammoniate is highly dependent on the material composition as well as the operation condition applied. In a general view, NH_3 evolution from metal amidoborane ammoniates remains a major concern but on the other hand, the incorporation of NH_3 as an additional H source does offer new possibilities for the development of high-capacity materials for generating molecular hydrogen. As a consequence, a substantial amount of effort has been devoted to the synthesis, characterization and property examination of novel metal amidoborane ammoniates. Quite recently, two approaches have been established for the synthesis of metal amidoborane ammoniates. One is the reaction of AB with metal amide/imide,[23,24] the other is a two-step procedure in which metal amidoborane was first prepared and then exposed to gaseous NH_3.[25] Our latest study found that directly mechanically milling the powder mixtures of AB and alkaline-earth metals or

[a]*Shenyang National Laboratory for Materials Science, Institute of Metal Research, Chinese Academy of Sciences, Shenyang, 110016, P. R. China. E-mail: pingwang@imr.ac.cn*
[b]*NIST Center for Neutron Research, National Institute of Standards and Technology, Gaithersburg, MD 20899-6102, USA. E-mail: huiwu@nist.gov*
[c]*Department of Materials Science and Engineering, University of Maryland, College Park, Maryland 20742-2115, USA*

† Electronic supplementary information (ESI) available: XRD and FTIR results of the post-milled MgH_2 under NH_3 atmosphere, the post-milled MgH_2 together with the liquid $AB(NH_3)_n$ complexes and the decomposition product(s) of $MgAB·3NH_3$. See DOI: 10.1039/c2jm31326j

their hydrides under NH_3 atmosphere can readily produce corresponding metal amidoborane ammoniates. In comparison with the existing approaches, the new approach is more straightforward and efficient. Particularly, the employment of a new approach may produce metal amidoborane ammoniate with an unusual coordination structure that is unobtainable using conventional methods. We herein report a case study of the preparation, structure and dehydrogenation property of $Mg(NH_2BH_3)_2(NH_3)_3$ (denoted as $MgAB\cdot3NH_3$) to demonstrate this new approach.

2. Experimental section

AB (97% purity) from Sigma-Aldrich[28] and MgH_2 (98% purity) from Alfa Aesar[28] were used as received. The AB–MgH_2 mixture in a molar ratio of 2 : 1 was mechanically milled under NH_3 atmosphere for 2 h by using a stainless steel vial (with a volume of around 60 cm^3) and balls (10 mm in diameter) in a Fritsch 7 Planetary mill at 400 rpm. The ball-to-powder weight ratio was around 100 : 1. To minimize the temperature increment in the vial, the ball milling was paused for 5 min after every 10 min of milling. In a typical run, the initial pressure of NH_3 in the milling vial was around 0.22 MPa. After ball milling, the vial was again connected to a vacuum line to measure the residual pressure inside. Then the gas was exposed to the ultra dry magnesium chloride ($MgCl_2$) (99.99% purity, Alfa Aesar, pretreated at 500 °C under a dynamic vacuum condition) followed by measurement of weight gain to determine the residual NH_3 amount in the milling vial. A similar procedure was also used for the determination of the NH_3 concentration in the gaseous decomposition products of $MgAB\cdot3NH_3$. All the sample handlings were performed in an argon (99.999% purity)-filled glovebox, which was equipped with a circulative purification system to maintain the H_2O/O_2 levels typically below 0.1 ppm.

The thermal decomposition behaviors of the samples were examined using TG/DSC/MS (Netzsch STA 449C Jupiter/QMS 403C). In a typical measurement run, the sample with a weight of about 3 mg was heated up to 300 °C at a ramping rate of 2 °C min^{-1}. In the thermal analyses measurements, high-purity argon (99.999%) was used as purge gas.

The TPD measurements were conducted in a carefully calibrated Sievert's type apparatus, typically under an initial pressure of <100 Pa. A precise pressure measurement was accomplished using a high-precision pressure transducer.

The samples in the as-prepared and post-heated states were characterized by XRD (Rigaku D/max 2500, Cu Kα radiation), FTIR (Bruker Tensor 27, 4 cm^{-1} resolution) and solid-state ^{11}B MAS NMR (Varian Infinityplus-400, operated at 9.4 T with a ^{11}B resonance frequency of 128.3 MHz). All the sample handlings were carried out in the argon-filled glovebox, and special measures were taken to minimize H_2O/O_2 contamination during the sample transferring processes. To minimize the H_2O/O_2 contamination during XRD examination, a polymer tape was used to cover the surface of the samples. The FTIR spectra were collected using the KBr-pellet method and the obtained spectra were normalized using OPUS 6.5 software. In the solid-state NMR measurements, solid samples were packed into a ZrO_2 rotor and spun at 12 kHz under nitrogen atmosphere. ^{11}B chemical shifts were referenced to solid $NaBH_4$ (−41 ppm). Proton decoupled, Bloch decay $^{11}B\{^1H\}$ experiments were run using a 3.5 μs 90° pulse, 64 kHz decoupling and a 10 s pulse delay. Each spectrum was accumulated for 16 scans.

3. Results and discussion

3.1 Reactive ball milling synthesis of $MgAB\cdot3NH_3$ and its crystal structure

In our previous effort to synthesize magnesium amidoborane ($Mg(NH_2BH_3)_2$) from ball-milling MgH_2 and AB,[29–31] we found that MgH_2 shows chemical inertness towards AB in the intensive mechanical milling process under Ar or H_2 atmosphere (Fig. 1(a)). Interestingly, the X-ray diffraction (XRD) pattern of the post-milled 2AB–MgH_2 sample under NH_3 atmosphere for 2 h completely changed with the disappearance of peaks from AB and only remnant peaks from MgH_2. Meanwhile, a new set of diffraction peaks was detected, which cannot be indexed to any known Mg–B–N–H quaternary compound. This result clearly indicates that a reaction occurred in the milling process with the presence of NH_3. The formation of the new compound was further confirmed by the solid-state magic-angle spinning nuclear magnetic resonance (MAS NMR) of $^{11}B\{^1H\}$. As presented in Fig. 2(a), the post-milled sample showed a single BH_3 resonance at −20.7 ppm, with a downfield shift of about 6 ppm compared with pristine AB (−26.5 ppm). A similar downfield shift of the BH_3 signal with respect to AB was also observed in amidoborane ammoniates such as $Mg(NH_2BH_3)_2(NH_3)$ ($MgAB\cdot NH_3$) and $Ca(NH_2BH_3)_2(NH_3)_2$ ($CaAB\cdot2NH_3$).[23,24] All these results suggest the formation of a new magnesium amidoborane ammoniate phase. In addition, monitoring the NH_3 change in the ball vial further confirmed its participation in the reaction during the milling process. The consumed amount of NH_3 was determined by measuring the pressure change in the ball vial before and after the milling process and the residual NH_3 amount in the ball vial after milling was examined using the ultra dry $MgCl_2$ adsorbent. These quantitative analyses indicated that AB–MgH_2–NH_3 should react in a stoichiometric ratio of 2 : 1 : 3 to form $MgAB\cdot3NH_3$ in the milling process following eqn (1).

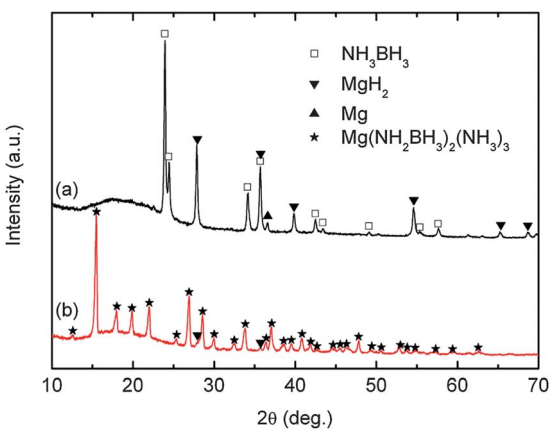

Fig. 1 Comparison of XRD patterns of 2AB–MgH_2 mixtures ball milled for 2 h under different atmospheres: (a) under Ar (or H_2) and (b) under NH_3.

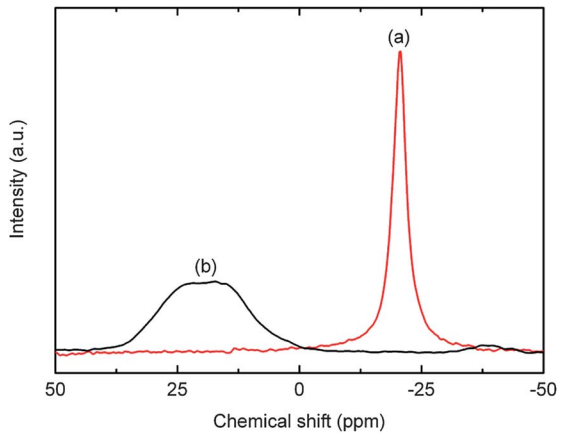

Fig. 2 $^{11}B\{^1H\}$ MAS NMR spectra of (a) the post-milled 2AB–MgH_2 sample under NH_3 atmosphere for 2 h; (b) the sample (a) after dehydrogenation up to 300 °C.

$$2NH_3BH_3(s) + MgH_2(s) + 3NH_3(g) \xrightarrow{\text{ball milling}} Mg(NH_2BH_3)_2(NH_3)_3(s) + 2H_2(g) \quad (1)$$

The speculated formula of the ammoniate product was subsequently confirmed by the structure determination. The XRD pattern of this new ammoniate phase (Fig. 1) can be indexed using a tetragonal structure with lattice parameters of approximately $a = 9.875$ Å and $c = 20.006$ Å. Assessment of the extinction symbol associated with the space group of the new phase indicated the most probable to be *P4/ncc*. The crystal structure was solved by direct-space methods under this space group. Due to the limited number of laboratory X-ray observations and the uncertain H positions, first-principles molecular dynamics simulated annealing calculations were then performed. Rietveld structural refinement on the optimal structural model was done using the GSAS package.[32] The $NH_2BH_3^-$ and NH_3 groups were kept as rigid bodies with the bond lengths and bond angles constrained as reasonable values due to the inadequate number of observations. Refinement of the cation position, rigid bodies, and lattice parameters ($a = 9.8908(5)$ Å and $c = 20.061(1)$ Å) yielded good agreement factors of $R_{wp} = 0.0594$ and $R_p = 0.0475$. The atomic positions from refinement are listed in Table S1 in ESI†, the Rietveld fit to the diffraction pattern is shown in Fig. 3, and the determined crystal structure is illustrated in Fig. 4.

A noticeable feature of the $Mg(NH_2BH_3)_2 \cdot 3NH_3$ structure is that Mg^{2+} exhibits both VI and IV coordinations, and in each coordination geometry Mg is surrounded only by the same type of ligands, leading to the formation of the $Mg(NH_2BH_3)_4^{2-}$ complex anion and the hexamminemagnesium(II) cation $Mg(NH_3)_6^{2+}$. This is quite distinct from the reported structure of $Mg(NH_2BH_3)_2 \cdot NH_3$ where Mg^{2+} shows solely IV coordinations and coordinates with three $(NH_2BH_3)^-$ groups and one NH_3 molecule simultaneously.[24] The $Mg(NH_2BH_3)_4^{2-}$ complex anion has been observed in the bimetallic amidoborane $Na_2Mg(NH_2BH_3)_4$,[22] where the formation of $Mg(NH_2BH_3)_4^{2-}$ was ascribed to the accommodation of the small but relatively highly charged Mg^{2+} to the large $NH_2BH_3^-$ anion. The Mg–N distances in $Mg(NH_2BH_3)_4^{2-}$ (2.25 Å) and in $Mg(NH_3)_6^{2+}$

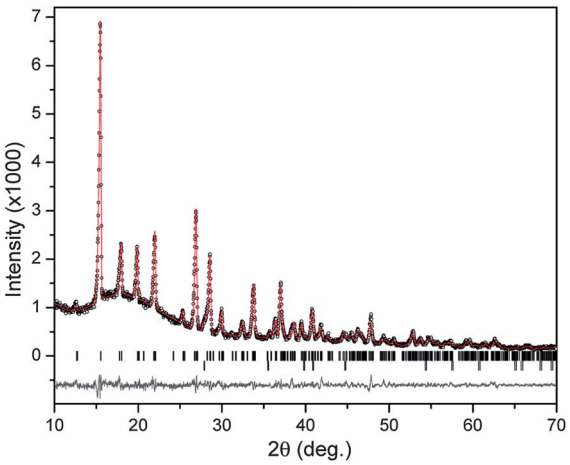

Fig. 3 Experimental (circles), calculated (line), and difference (line below observed and calculated patterns) XRD profiles for $Mg(NH_2BH_3)_2(NH_3)_3$ at 298 K. Vertical bars indicate the calculated positions of Bragg peaks of $Mg(NH_2BH_3)_2(NH_3)_3$ (98.05(8) wt%) and MgH_2 (1.95(8) wt%), respectively (from the top).

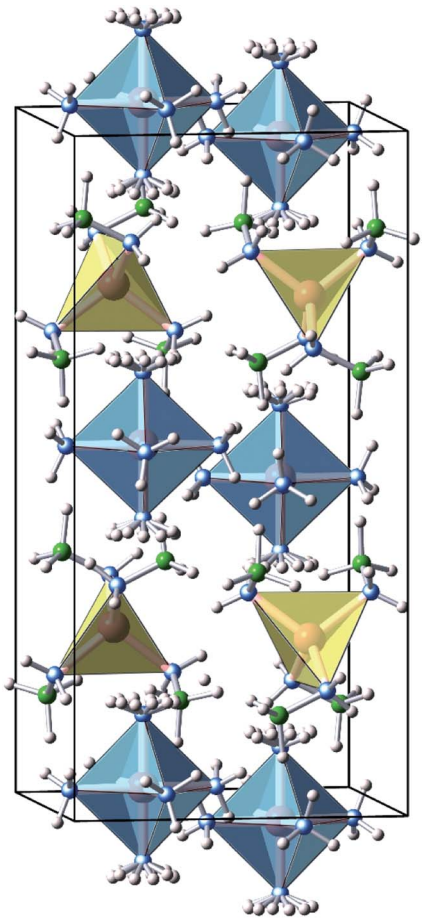

Fig. 4 Crystal structure of $Mg(NH_2BH_3)_2(NH_3)_3$ with ordering of the $Mg[NH_2BH_3]_4^{2-}$ tetrahedra (highlighted in yellow) and $Mg[NH_3]_6^{2+}$ octahedra (in blue). Mg, B, N and H atoms are represented by pink, green, blue and white spheres, respectively. Note: the H's in the NH_3 molecules of the 4*c* positions (above and below Mg atoms) are orientationally disordered.

(2.16–2.24 Å) are consistent with those in $Na_2Mg(NH_2BH_3)_4$ and the hexamminemagnesium salts such as $Mg(NH_3)_6Cl_2$ halides. The $Mg(NH_3)_6^{2+}$ octahedra and $Mg(NH_2BH_3)_4^{2-}$ tetrahedra were spread along the *ab*-basal plane, respectively, leading to the formation of the oppositely charged cationic and anionic layers. As a result, different coordination preferences of Mg^{2+} drives the compound to adopt an intriguing 1 : 1 ordered structure with alternating layers of $Mg(NH_2BH_3)_4^{2-}$ anions and $Mg(NH_3)_6^{2+}$ cations (Fig. 4). Such ordering in both cation coordination and ligand type is in sharp contrast to any other metal amidoborane ammoniates. The ligand and cation coordination ordering was also observed in the recently reported $Li_2Al(BH_4)_5 \cdot 6NH_3$,[33] whereas in that case the ordering is driven by the coordination preferences of two different cations (*i.e.*, Li and Al). The coordination ordering from the same type of cation is common in oxides such as the famous brownmillerite-type ferrites. However, to the best of our knowledge, the structural ordering caused by the various coordinations of the same cation type is only observed in $Mg(NH_2BH_3)_2 \cdot 3NH_3$ thus far for all known complex hydrides.

Notably, the newly developed ball-milling reaction approach can also be employed to prepare other amidoborane ammoniates. For example, mechanically milling the 2AB–CaH_2 mixture under NH_3 atmosphere resulted in the formation of $CaAB \cdot 2NH_3$. In addition, it was found that using Mg powder instead of MgH_2 to react with AB and gaseous NH_3 under an identical milling condition can also produce $MgAB \cdot 3NH_3$.

3.2 Formation mechanism of $MgAB \cdot 3NH_3$

A series of control experiments have been conducted to gain insight into the formation mechanism of $MgAB \cdot 3NH_3$. As AB does not react with MgH_2 under normal milling conditions (Ar or H_2 atmosphere), our preliminary study mainly focused on the determination of the possible reactive intermediates formed *via* the solid–gas reactions between NH_3 and individual MgH_2 or AB. According to the literature, MgH_2 can react with gaseous NH_3 to form $Mg(NH_2)_2$ and ball-milling a 2AB–$Mg(NH_2)_2$ powder mixture can produce $MgAB \cdot NH_3$.[24,34] To check the possibility of this mechanistic pathway, we first solely milled the MgH_2 powders under identical conditions as for the preparation of $MgAB \cdot 3NH_3$. XRD analysis of the post-milled sample found that the diffraction peaks of MgH_2 became significantly weakened and broadened, which is consistent with the literature results (Fig. S1, ESI†). But according to the parallel Fourier transformation infrared (FTIR) spectroscopy analysis, only a small amount of $Mg(NH_2)_2$ was formed under the current milling conditions (Fig. S2, ESI†). This finding, together with the observed rapid formation of $MgAB \cdot 3NH_3$ in the AB–MgH_2–NH_3 mixture, suggests that the formation of $MgAB \cdot 3NH_3$ may not necessarily involve the $Mg(NH_2)_2$ intermediate. On the other hand, our study found that reducing the NH_3 amount in the milling process exerts little influence on the ammoniate product species, *i.e.*, no $MgAB \cdot NH_3$ but only $MgAB \cdot 3NH_3$ phase and extra MgH_2 precursor residue were detected in the XRD pattern of a post-milled 2 : 1 : 2 AB–MgH_2–NH_3 sample. Furthermore, it was found that mechanically ball milling $MgAB \cdot NH_3$ under NH_3 atmosphere cannot lead to the formation of $MgAB \cdot 3NH_3$ (Fig. S3, ESI†). All these results suggest that a reaction pathway *via* the intermediate $Mg(NH_2)_2$ and $MgAB \cdot NH_3$ can be excluded in the formation of $MgAB \cdot 3NH_3$ using the current preparation method.

The solid–gas reaction between AB and NH_3 and its possible correlation to the formation of $MgAB \cdot 3NH_3$ were also investigated. Our study found that the AB powders rapidly convert to a liquid substance after exposure to 2 bars of NH_3 for several minutes at room temperature. This finding agrees well with the latest report by Gao *et al.*, which demonstrated that AB can readily absorb NH_3 to form liquid $AB(NH_3)_n$ (n = 1–6) complexes.[35] Our control experiment showed that mechanically milling MgH_2 powder with the liquid $AB(NH_3)_n$ complexes results in the rapid formation of $MgAB \cdot 3NH_3$ (Fig. S4, ESI†). Apparently, in comparison with the solid AB, the liquid $AB(NH_3)_n$ complexes show increased reactivity towards MgH_2. Therefore, the formation of $AB(NH_3)_n$ intermediate under NH_3 atmosphere should be a key mechanistic step in the reactive ball-milling synthesis of $MgAB \cdot 3NH_3$.

3.3 Thermal decomposition behaviors of $MgAB \cdot 3NH_3$

Fig. 5 presents the synchronous thermogravimetry/differential scanning calorimetry/mass spectroscopy (TG/DSC/MS) results of the as-prepared $MgAB \cdot 3NH_3$ sample. It was observed that $MgAB \cdot 3NH_3$ starts to decompose from around 50 °C, and reaches its maximum dehydrogenation rate at 83 °C. The major dehydrogenation step in the temperature range of 60–120 °C is an exothermic event. The thermolysis is similar to that of $MgAB \cdot NH_3$.[24] The total weight loss from the sample reaches up to 26 wt% upon heating to 300 °C. According to the MS results, the H_2 release from $MgAB \cdot 3NH_3$ is accompanied with the

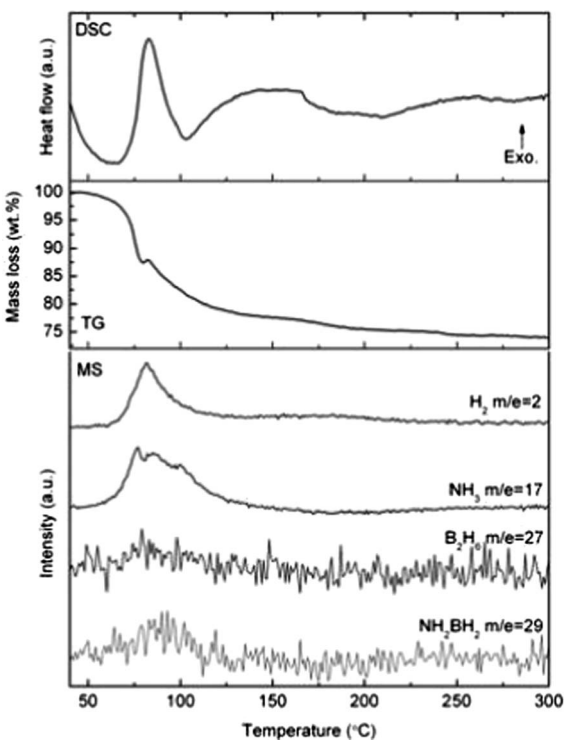

Fig. 5 TG/DSC/MS profiles of $MgAB \cdot 3NH_3$. The ramping rate is 2 °C min^{-1}.

evolution of a significant amount of NH_3 and trace amounts of diborane (B_2H_6) and monomeric aminoborane (NH_2BH_2), which accounts for the large fraction of the total weight loss. In contrast, only a small amount of NH_3 other than H_2 was reported to be released from the $MgAB \cdot NH_3$ decomposition.[24] This difference in the released NH_3 amount may arise from the more large protonic H(N) to hydridic H(B) ratio in the $MgAB \cdot 3NH_3$ relative to the $MgAB \cdot NH_3$, leading to the incomplete conversion of NH_3 to H_2 in the dehydrogenation process.

The decomposition behavior of $MgAB \cdot 3NH_3$ was further examined using a volumetric method. Fig. 6 shows a temperature-programmed desorption (TPD) profile of the $MgAB \cdot 3NH_3$ sample. It was found that the decomposition of $MgAB \cdot 3NH_3$ in a closed system yields much less NH_3 than that in dynamic Ar flow. This is in accord with the decomposition properties of other metal amidoborane ammoniates,[23,24] indicating the participation of most of the NH_3 in the dehydrogenation reaction in a quasi-equilibrium condition. A quantitative measurement using an ultra dry $MgCl_2$ adsorbent determined that the NH_3 concentration that can survive in the gas phase in a closed system is around 2 mol%. If ignoring the small contribution from NH_3 contaminant, the desorbed hydrogen amounts to up to 10.6 wt% upon heating to 300 °C. This value corresponds to 7 equivalents of H_2 per $MgAB \cdot 3NH_3$, which is higher than the expected 6 equivalents of H_2 from the combination of $H^{\delta-}$(B) and $H^{\delta+}$(N) that was reported for the dehydrogenation of $MgAB \cdot NH_3$ or $CaAB \cdot 2NH_3$.[23,24] Although the mechanism underlying the excessive H_2 release remains unclear, it is likely that this difference may come from the unique coordination structure of $MgAB \cdot 3NH_3$. Nevertheless, on the basis of the TPD result, the dehydrogenation reaction can be roughly described by eqn (2).

$$Mg(NH_2BH_3)_2(NH_3)_3 \rightarrow MgN_5B_2H_5 + 7H_2 \qquad (2)$$

The dehydrogenation product(s) with a nominal formula of $MgN_5B_2H_5$ were characterized by a combination of XRD/FTIR/NMR techniques. XRD revealed a poorly crystalline product and a small amount of MgH_2, which should be assigned to the unreacted precursor residue in preparation of $MgAB \cdot 3NH_3$ (Fig. S5, ESI†). The ^{11}B NMR spectrum of the product(s) (Fig. 2(b)) showed at least two overlapped resonances centered at around 22.7 and 15.5 ppm, indicating the presence of boron species in the tri-coordinated BN_3 or BN_2H environments. Similar results have been reported for the products of $CaAB \cdot 2NH_3$.[23] However, only a single boron resonance at 29 ppm was observed for the post-dehydrogenated $MgAB \cdot NH_3$ sample by high-field ^{11}B NMR.[24] In addition, a weak and broad ^{11}B signal was also observed at around −38 ppm, suggesting the presence of a small amount of tetracoordinated B species. FTIR results show a weak B–H stretching band and smearing of N–H modes in NH_3 and NH_2 (Fig. S6, ESI†), indicating the consumption of BH_3 and NH_3 or NH_2 during dehydrogenation. In contrast, Chen *et al.* reported that only sp^2 boron resonances and N–H stretching bands were observed for the decomposition products of its $MgAB \cdot NH_3$ and $CaAB \cdot 2NH_3$ analogues by the ^{11}B NMR and FTIR spectra examinations, respectively.[23,24] On the basis of these results, it may be deduced that the amount of adducted NH_3 and/or coordination structures may exert a substantial influence on the decomposition pathway and products.

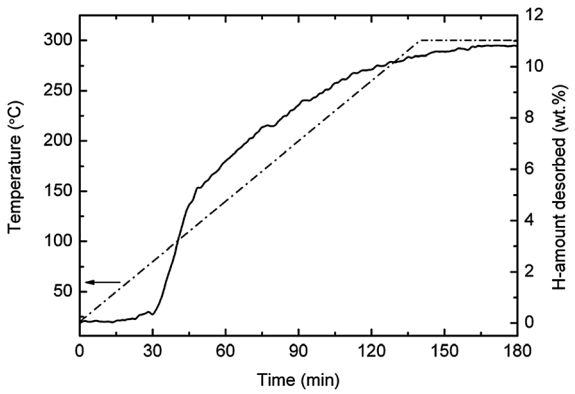

Fig. 6 TPD profile of $MgAB \cdot 3NH_3$. The ramping rate is 2 °C min^{-1}.

$MgAB \cdot 3NH_3$ is a new member of the metal amidoborane ammoniate family. In comparison with its $MgAB \cdot NH_3$ and $CaAB \cdot 2NH_3$ analogues, $MgAB \cdot 3NH_3$ exhibits a completely different crystal structure but similar decomposition behaviors in general. Better understanding of its structure–property correlation may provide valuable insight into the structure–composition design of novel multi-component compounds for potential hydrogen storage application.

4. Conclusions

Mechanically milling the stoichiometric mixture of ammonia borane and magnesium hydride under ammonia atmosphere can readily produce a new magnesium amidoborane ammoniate, $Mg(NH_2BH_3)_2(NH_3)_3$ ($MgAB \cdot 3NH_3$). A combination of XRD analysis and first-principles calculations determined that $MgAB \cdot 3NH_3$ adopts an unusual crystal structure with ordering in both cation coordination and ligand arrangement, and contains $Mg(NH_3)_6^{2+}$ complex cation and $Mg(NH_2BH_3)_4^{2-}$ complex anion. $MgAB \cdot 3NH_3$ can release 7 equivalents (10.6 wt %) of H_2 up to 300 °C in a closed system. In the open system the H_2 release from $MgAB \cdot 3NH_3$ is accompanied with the evolution of NH_3. $MgAB \cdot 3NH_3$ is just the first example that demonstrates the viability of the reactive ball-milling approach. In comparison with the conventional methods, this newly developed approach appears more straightforward and efficient. Furthermore, as the new approach involves the formation of more reactive $AB(NH_3)_n$ as a key intermediate, it is expected that this approach can be employed for synthesizing other metal amidoborane ammoniates or related materials.

Acknowledgements

The financial support for this research from the National Basic Research Program of China (2010CB631305), the National High-Tech R&D Program of China (2009AA05Z109), the National Outstanding Youth Science Foundation of China (51125003), the National Natural Science Foundation of China (50801059), and the Main Direction Program of Knowledge Innovation of CAS (KGCXZYW-342) are gratefully acknowledged.

Notes and references

1 L. Schlapbach and A. Zuttel, *Nature*, 2001, **414**, 353–358.
2 G. Wolf, J. Baumann, F. Baitalow and F. P. Hoffmann, *Thermochim. Acta*, 2000, **343**, 19–25.
3 F. H. Stephens, V. Pons and R. T. Baker, *Dalton Trans.*, 2007, 2613–2626.
4 P. Wang, *Dalton Trans.*, 2012, **41**, 4296–4302.
5 A. Gutowska, L. Y. Li, Y. S. Shin, C. M. M. Wang, X. H. S. Li, J. C. Linehan, R. S. Smith, B. D. Kay, B. Schmid, W. Shaw, M. Gutowski and T. Autrey, *Angew. Chem., Int. Ed.*, 2005, **44**, 3578–3582.
6 A. Feaver, S. Sepehri, P. Shamberger, A. Stowe, T. Autrey and G. Z. Cao, *J. Phys. Chem. B*, 2007, **111**, 7469–7472.
7 L. Li, X. Yao, C. H. Sun, A. J. Du, L. N. Cheng, Z. H. Zhu, C. Z. Yu, J. Zou, S. C. Smith, P. Wang, H. M. Cheng, R. L. Frost and G. Q. M. Lu, *Adv. Funct. Mater.*, 2009, **19**, 265–271.
8 S. Gadipelli, J. Ford, W. Zhou, H. Wu, T. J. Udovic and T. Yildirim, *Chem.–Eur. J.*, 2011, **17**, 6043–6047.
9 D. J. Heldebrant, A. Karkamkar, N. J. Hess, M. Bowden, S. Rassat, F. Zheng, K. Rappe and T. Autrey, *Chem. Mater.*, 2008, **20**, 5332–5336.
10 D. W. Himmelberger, C. W. Yoon, M. E. Bluhm, P. J. Carroll and L. G. Sneddon, *J. Am. Chem. Soc.*, 2009, **131**, 14101–14110.
11 D. Neiner, A. Karkamkar, J. C. Linehan, B. Arey, T. Autrey and S. M. Kauzlarich, *J. Phys. Chem. C*, 2009, **113**, 1098–1103.
12 S. B. Kalidindi, J. Joseph and B. R. Jagirdar, *Energy Environ. Sci.*, 2009, **2**, 1274–1276.
13 J. H. Luo, X. D. Kang, Z. Z. Fang and P. Wang, *Dalton Trans.*, 2011, **40**, 6469–6474.
14 Y. S. Chua, P. Chen, G. T. Wu and Z. T. Xiong, *Chem. Commun.*, 2011, **47**, 5116–5129.
15 Z. T. Xiong, C. K. Yong, G. T. Wu, P. Chen, W. Shaw, A. Karkamkar, T. Autrey, M. O. Jones, S. R. Johnson, P. P. Edwards and W. I. F. David, *Nat. Mater.*, 2008, **7**, 138–141.
16 X. D. Kang, Z. Z. Fang, L. Y. Kong, H. M. Cheng, X. D. Yao, G. Q. Lu and P. Wang, *Adv. Mater.*, 2008, **20**, 2756–2759.
17 H. Wu, W. Zhou and T. Yildirim, *J. Am. Chem. Soc.*, 2008, **130**, 14834–14839.
18 H. V. K. Diyabalanage, T. Nakagawa, R. P. Shrestha, T. A. Semelsberger, B. L. Davis, B. L. Scott, A. K. Burrell, W. I. F. David, K. R. Ryan, M. O. Jones and P. P. Edwards, *J. Am. Chem. Soc.*, 2010, **132**, 11836–11837.
19 Q. A. Zhang, C. X. Tang, C. H. Fang, F. Fang, D. L. Sun, L. Z. Ouyang and M. Zhu, *J. Phys. Chem. C*, 2010, **114**, 1709–1714.
20 X. D. Kang, J. H. Luo, Q. A. Zhang and P. Wang, *Dalton Trans.*, 2011, **40**, 3799–3801.
21 K. J. Fijalkowski, R. V. Genova, Y. Filinchuk, A. Budzianowski, M. Derzsi, T. Jaron, P. J. Leszczynski and W. Grochala, *Dalton Trans.*, 2011, **40**, 4407–4413.
22 H. Wu, W. Zhou, F. E. Pinkerton, M. S. Meyer, Q. R. Yao, S. Gadipelli, T. J. Udovic, T. Yildirim and J. J. Rush, *Chem. Commun.*, 2011, **47**, 4102–4104.
23 Y. S. Chua, G. T. Wu, Z. T. Xiong, T. He and P. Chen, *Chem. Mater.*, 2009, **21**, 4899–4904.
24 Y. S. Chua, G. T. Wu, Z. T. Xiong, A. Karkamkar, J. P. Guo, M. X. Jian, M. W. Wong, T. Autrey and P. Chen, *Chem. Commun.*, 2010, **46**, 5752–5754.
25 G. L. Xia, X. B. Yu, Y. H. Guo, Z. Wu, C. Z. Yang, H. K. Liu and S. X. Dou, *Chem.–Eur. J.*, 2010, **16**, 3763–3769.
26 H. Wu, W. Zhou, F. E. Pinkerton, M. S. Meyer, G. Srinivas, T. Yildirim, T. J. Udovic and J. J. Rush, *J. Mater. Chem.*, 2010, **20**, 6550–6556.
27 A. Klerke, C. H. Christensen, J. K. Nørskov and T. Vegge, *J. Mater. Chem.*, 2008, **18**, 2304–2310.
28 Certain commercial suppliers are identified in this paper to foster understanding. Such identification does not imply recommendation or endorsement by the NIST, nor does it imply that the materials or equipment identified are necessarily the best available for the purpose.
29 X. D. Kang, L. P. Ma, Z. Z. Fang, L. L. Gao, J. H. Luo, S. C. Wang and P. Wang, *Phys. Chem. Chem. Phys.*, 2009, **11**, 2507–2513.
30 J. H. Luo, X. D. Kang and P. Wang, *ChemPhysChem*, 2010, **11**, 2152–2157.
31 J. H. Luo, X. D. Kang and P. Wang, *J. Phys. Chem. C*, 2010, **114**, 10606–10611.
32 A. C. Larson and R. B. Von Dreele, *General Structure Analysis System*, Report LAUR 86-748, Los Alamos National Laboratory, NM, 1994.
33 Y. H. Guo, H. Wu, W. Zhou and X. B. Yu, *J. Am. Chem. Soc.*, 2011, **133**, 4690–4693.
34 H. Y. Leng, T. Ichikawa, S. Hino, N. Hanada, S. Isobe and H. Fujii, *J. Power Sources*, 2006, **156**, 166–170.
35 L. Gao, H. C. Fang, Z. H. Li, X. B. Yu and K. N. Fan, *Inorg. Chem.*, 2011, **50**, 4301–4306.